Turkish Journal of Chemistry

http://journals.tubitak.gov.tr/chem/

Research Article

Turk J Chem
(2015) 39: 359 – 371

doi:10.3906/kim-1407-24

Selective CO methanation over $NiO–Al_2O_3–ZrO_2$ and $Co_3O_4–Al_2O_3–ZrO_2$ catalysts

Filiz BALIKÇI DEREKAYA*, Derya MERCAN ERMERGEN
Advanced Technologies Department, Graduate School of Natural and Applied Sciences, Gazi University, Ankara, Turkey

Received: 08.07.2014 • **Accepted/Published Online:** 11.12.2014 • **Printed:** 30.04.2015

Abstract: $NiO–Al_2O_3–ZrO_2$ and $Co_3O_4–Al_2O_3–ZrO_2$ catalysts were prepared by three different co-precipitation methods, namely co-precipitation, surfactant-assisted co-precipitation, and surfactant-assisted co-precipitation with ultrasound mixing methods, and their activities were tested in selective CO methanation. Catalysts were characterized using N_2 physisorption, XRD, SEM, TEM, XPS, and TPR-H_2 techniques. CO methanation and selective CO methanation reactions were carried out. Catalysts prepared by surfactant assisted co-precipitation gave high surface area, uniform pore size distributions, and small pores. The $NiO–Al_2O_3–ZrO_2$ catalyst prepared by surfactant-assisted co-precipitation gave 50% CO conversion to CH_4 at 155 °C and all CO converted to CH_4 when T > 225 °C. For the selective CO methanation, the CO level decreased below 100 ppm at 200 °C over the $NiO–Al_2O_3–ZrO_2$ catalyst prepared by surfactant-assisted co-precipitation.

Key words: Surfactant, ultrasound, Al_2O_3-ZrO_2, methanation

1. Introduction

The $H_2–CO–CO_2$ gas mixture is produced from steam reforming of hydrocarbons, naphtha, and coal gasification processes. This gas mixture has been widely used to produce town gas and useful chemicals. However, the $H_2–CO–CO_2$ gas mixture has some negative features, like containing poisonous CO. If CO is converted to CH_4, a gas mixture that involves higher energy can be obtained.[1,2] The main carbon containing components of the syngas are CO and CO_2. Therefore, methane can be produced by the hydrogenation of CO and CO_2 by the following equations:

$$CO + 3H_2 \rightarrow CH_4 + H_2O \quad (1)$$

$$CO_2 + 4H_2 \rightarrow CH_4 + 2H_2O \quad (2)$$

Ni-based catalysts were mostly used for the methanation reaction.[3–5] However, activities of Ni-based catalysts tend to decrease catalyst deactivation because of carbon deposition and sintering, which lead to the reduction of the Ni active sites.[3] When Ni was prepared with Al_2O_3, Ni sintering was decreased.[3,6,7] Methanation was studied over the $Ni–Al_2O_3$ catalyst in several studies.[8,9] These studies revealed that CO methanation was dependent mostly on Ni in the catalyst structure. According to Chen et al., carbon monoxide adsorbs on reduced nickel and transfers to Al_2O_3 to form H–CO complex during the methanation of CO.[9] Zhao et al. also supported this conclusion. They observed that syngas methanation over Ni/Al_2O_3 catalysts was sensitive to Ni

*Correspondence: filizb@gazi.edu.tr

particle size and Ni loadings.[3] Cobalt containing catalysts were used for different types of reactions (Fischer–Tropsch synthesis, NOx removal, partial oxidation of olefins, hydrodesulfurization, CO oxidation, etc.) due to their redox properties. High dispersion of the cobalt on the support leads to improved catalyst activity and stability over the supported cobalt containing catalysts.[10–14] CO methanation was studied also over Co_3O_4 based catalysts.[1,6,10–16] Zhu et al. studied CO methanation over nanosized Co_3O_4 that had different particle sizes. They observed that activity of catalysts increased with decreasing particle size and gas hourly space velocity.[17] Co_3O_4 leads to improvement in the catalyst surface area and the porous structure.[18,19] CeO_2 has been used as promoter for Ni catalysts since it improves the thermal stability of alumina, promotes Ni dispersion, and changes the properties of Ni.[6] In the present study, methanation was studied over the NiO–Al_2O_3–ZrO_2 and Co_3O_4–Al_2O_3–ZrO_2 catalysts. The ZrO_2 improves the catalysts' thermal stability[13–21] and Al_2O_3 inhibits Ni sintering.[8] The effect of ZrO_2 on Ni/Al_2O_3 and Co_3O_4/Al_2O_3 for CO methanation has not been studied yet. The ZrO_2–Al_2O_3 catalyst support has high surface area, basicity, and thermal stability. The effect of ZrO_2 on the Ni/Al_2O_3 catalyst was investigated for CO_2 methanation, and it was indicated that the presence of ZrO_2 improved the catalytic activity and stability of CO_2 methanation.[22]

The catalyst preparation method has great effect on the characteristic and catalytic properties of the catalyst. In the present study we used three different methods based on precipitation. The first is traditional co-precipitation, the second is surfactant-assisted co-precipitation, and the third is surfactant-assisted co-precipitation with ultrasound mixing. Addition of surfactant to the catalyst preparation leads to an increase in the catalytic activity of the final catalyst, since the final catalyst has smaller crystallite size, higher surface area, and greater adsorption capacity.[23,24] The parameters and conditions (pH, temperature, mixing media, etc.) that are used in the catalyst preparation are very important. In this catalyst ultrasound mixing was used during the preparation step. According to previous studies, ultrasound is a useful technique in which at the end of preparation the final catalyst has homogeneous particle size distribution and high surface area and active metal sizes are smaller. Therefore, we have more active and stable catalysts.[25,26]

The aim of the present study was to develop a catalyst that shows high activity for CO methanation and selective CO methanation reactions. For this aim, two different catalysts were prepared as follows: 50/25/25 (mol %) NiO–Al_2O_3–ZrO_2 and 50/25/25 (mol %) Co_3O_4–Al_2O_3–ZrO_2. The catalysts were prepared by using three different co-precipitation methods. All three methods are based on precipitation but the procedures are different. The methods were called (1) co-precipitation (C), (2) surfactant-assisted co-precipitation (S), and (3) surfactant-assisted co-precipitation with ultrasound mixing (U). The resultant effects of the surfactant and ultrasound were determined. (In the text given below NiAlZr and CoAlZr are used instead of NiO–Al_2O_3–ZrO_2 and Co_3O_4–Al_2O_3–ZrO_2, respectively.)

2. Results and discussion

2.1. Catalyst characterization results

Figure 1 shows the XRD spectra collected from all catalysts after calcination. The CoAlZr catalyst shows diffraction peaks, which were due to the CoO, Co_3O_4, Al_2O_3, ZrO_2, and $CoAl_2O_4$ crystal phases. The CoO peak was observed at $2\theta = 18.17^\circ$. The Co_3O_4 peaks were observed at $2\theta = 31.03^\circ$, 36.03°, 44.31°, 58.51°, and 64.48°. The $CoAl_2O_4$ peaks were observed at $2\theta = 55.51^\circ$ and 68.62°. The CoAlZr–S and CoAlZr–U catalysts show ZrO_2 diffraction peaks at $2\theta = 74.13^\circ$. The CoAlZr–C catalyst shows ZrO_2 diffraction peaks at $2\theta = 51.37^\circ$ and 74.13°. The Al_2O_3 peaks were observed at $2\theta = 38.62^\circ$ and 68.62°. The NiAlZr catalysts

show diffraction peaks that were due to the NiO, ZrO_2, and $NiAl_2O_4$ crystal phases. The NiO peaks were observed at $2\theta = 43.20°$ and $62.75°$. The $NiAl_2O_4$ peaks were observed at $2\theta = 37.24°$ and $43.20°$. The NiAlZr–S and NiAlZr–U gave ZrO_2 diffraction peaks at $2\theta = 75.17°$ and $79.37°$. The NiAlZr–C catalyst show ZrO_2 diffraction peaks at $2\theta = 30.34°$, $50.62°$, $75.17°$, and $79.37°$. The peaks responsible for the NiO phase and ZrO_2 phase were in accordance with the literature.[27–29]

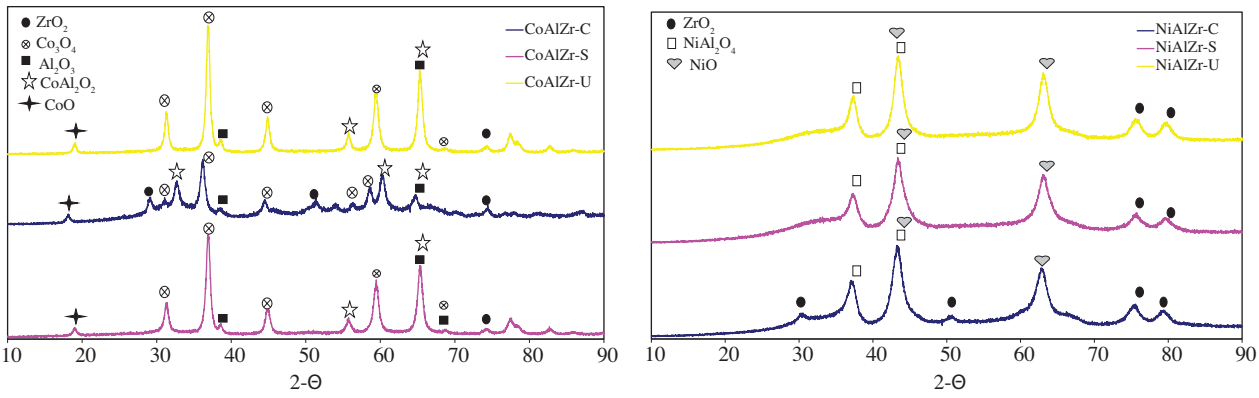

Figure 1. XRD diagrams of the catalysts.

Average crystallite sizes of the catalysts are listed in Table 1. The average crystallite sizes of the CoAlZr catalysts and NiAlZr catalysts were calculated over the diffraction peak due to Co_3O_4 ($2\theta = 36.2°$) and NiO ($2\theta = 43.7°$) by using the Debye–Scherrer equation, respectively. A decrease in Co_3O_4 average crystallite size was observed by changing the preparation method. The smallest crystallite size of Co_3O_4 was obtained from the CoAlZr–U catalyst. The ultrasonic mixing affected the average crystallite size of Co_3O_4. All NiAlZr catalysts gave the same average crystallite size. Changing the preparation method did not affect the average crystallite size of the NiAlZr catalysts.

Table 1. Textural and structural properties of the catalysts.

Catalysts	Surface area m^2/g			$V_{micro+meso}$ pore volume (liquid N_2 cc/g)			V_{total} pore volume (liquid N_2 cc/g)			Average pore diameter (nm)			Average crystallite size (nm)		
	Preparation methods														
	C[3]	S[4]	U[5]	C	S	U	C	S	U	C	S	U	C	S	U
CoAlZr[1]	83	94	92	0.353	0.335	0.441	0.372	0.483	0.496	2.1, 5.5, 27.6	2.1, 3.8, 9.6, 30.3	3.0, 4.8, 6.5, 31.5	5	4.2	3.9
NiAlZr[2]	146	204	150	0.242	0.346	0.270	0.257	0.364	0.282	4.9	3.8, 6.6	3.8, 6.5	2	2	2

[1]: Co_3O_4–Al_2O_3–ZrO_2, [2]: NiO–Al_2O_3–ZrO_2, [3]: Co-precipitation, [4]: Surfactant

Nitrogen adsorption desorption isotherms of the catalysts were obtained from the N_2 physisorption analysis (see Figure 2). Catalysts showed different hysteresis behaviors. According to the IUPAC classification Type IV and Type V adsorption isotherms were obtained. The CoAlZr–C showed a Type V adsorption desorption isotherm. A Type V isotherm was obtained from porous adsorbents. The CoAlZr–S, CoAlZr–U, and NiAlZr prepared by the three different methods showed Type IV adsorption desorption isotherms. This type of isotherm is obtained from mesoporous adsorbents.[30] According to the shape of the hysteresis, the shape of the structure can be estimated. Catalysts prepared by co-precipitation showed Type H3 hysteresis, which was observed with aggregates at plate-like particles giving rise to slit-shaped pores. Catalysts prepared by the

S and U method showed Type H2 hysteresis, indicating the existence of cylindrical mesopores in the prepared material.[31] According to the type of adsorption isotherm, it can be estimated that the highest catalytic activity may be observed from the catalysts that show Type IV adsorption isotherms.

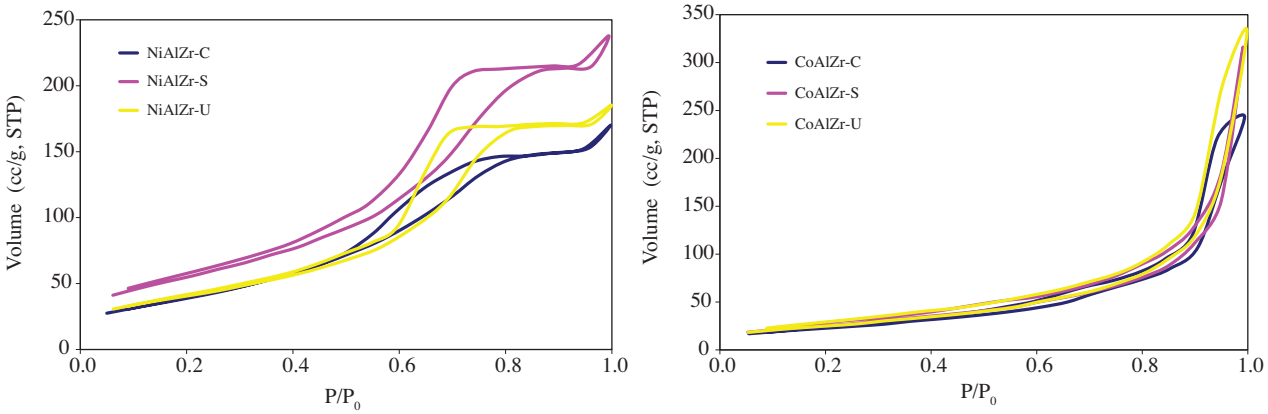

Figure 2. N_2 adsorption/desorption isotherms of the catalysts.

Table 1 shows the multipoint BET surface areas of the catalyst. The results revealed that the preparation method has an important effect on the surface area of the catalyst. The surface area values are arranged depending on the preparation method: S > U > C. The results indicated that the most effective parameter in the preparation method is using a surfactant. By using a surfactant, the phase structure and morphology can be controlled.[32,33] Moreover, catalysts prepared by using the surfactant have narrow and monomodal pore size distribution.[34] These results indicated that high activity for the methanation reaction would be obtained with catalysts prepared by the S and U methods. The average pore sizes of the catalysts are listed in Table 1. All catalysts have mesopores (2 nm < d < 50 nm). Pore sizes of the catalysts varied with the preparation method type. The surfactant and ultrasound have significant effects on the pore sizes of the catalysts. Smaller pore sizes and more uniform pore size distributions were obtained with the S and U methods.

XPS analysis of the CoAlZr catalyst showed that the binding energies of the Al 2p, Al 2s, Co 2p, Zr 3d, and O 1s lines were in agreement with the literature.[32,35–37] The Co 2p 3/2 binding energies were measured as 778.1 eV, 778.8 eV, and 779.3 eV. The Co 2p1/2 binding energies were measured as 793.8 eV and 794.4 eV. According to these results, cobalt was present in the catalyst structure as Co_3O_4 crystal phase.[32] The Zr 3d 3/2 peaks were observed between 180.3 and 181 eV and Zr 3d3/2 binding energies were measured as 183.2 eV and 182.8 eV, which were consistent with the ZrO_2 phase.[35] Al 2p binding energy was observed as 72.92 eV. In the literature, the binding energy of Al 2p was 74.6 eV.[36] This difference was due to the catalyst compositions. The O 1s binding energies were 528.6 eV, 529.1 eV, and 529 eV due to the lattice oxygen in the metal oxide structure.[35] XPS analysis of the NiAlZr catalysts showed peaks due to Zr 3d, Al 2p, Al 2s, O 1s, and Ni 2p. The Zr 3d5/2 binding energies were 180.5 eV, 180.8 eV, and 181.2 eV. The Zr 3d7/2 binding energies were 183 eV, 183.2 eV, and 183.4 eV. The Al 2p binding energies were 72.82 eV and 73 eV. The O 1s binding energies were 528 eV, 529 eV, and 529.6 eV. The Ni 2p3/2 peak was observed between 853.8 and 855.2 eV of which the satellite peak was connected at 860 eV. The Ni 2p1/2 peak was observed between 871.9 and 872.2 eV of which the satellite peak was connected at 878 eV. According to the results, Ni was in the form of NiO in the catalyst structures[37] and Zr was in the form of ZrO_2 in the catalyst structure.[35]

Temperature programmed reduction studies were carried out in order to determine the reduction temperatures of the catalysts. Since hydrogen existed in the reaction gas mixture, the behavior of the catalyst against the hydrogen was determined by using the TPR technique. TPR–H_2 results of the NiAlZr catalysts are shown in Figure 3. The area under the TPR–H_2 curves of the catalysts are very close to each other and the shapes of the curves are very similar. This similarity might be due to the reduction of only the NiO phase in the catalyst structure. Among the catalysts, NiAlZr–U catalyst began to be reduced at a higher temperature than NiAlZr–C and NiAlZr–S catalysts. The NiAlZr–U catalyst was the most resistant catalyst among the NiAlZr catalysts. The NiAlZr–C, NiAlZr–S, and NiAlZr–U gave reduction peaks at 473 °C, 493 °C, and 591 °C, respectively. The low temperature reduction peaks were due to the reduction of NiO, which was supported by the literature.[38] The TPR–H_2 profiles of the CoAlZr catalysts are shown in Figure 3. The CoAlZr–C catalyst gave reduction peaks at 340 °C, 494 °C, and 580 °C. The CoAlZr–S catalyst gave reduction peaks at 382 °C and 666 °C. The CoAlZr–U catalyst gave reduction peaks at 382 °C, 502 °C, and 734 °C. The low temperature reduction peak was due to the reduction of Co_3O_4 to CoO.[39,40] The high temperature reduction peak was due to the reduction of CoO to Co.[39,40] The reduction peaks obtained at 494 °C and 502 °C might be due to the reduction of O_2 in the ZrO_2 structure.[39,40] Because of the interaction between Al_2O_3 and ZrO_2, the high temperature reduction peaks obtained from the CoAlZr–U and CoAlZr–S catalysts shifted to higher temperatures. These results showed that catalysts prepared with the surfactant have high resistance against H_2 reduction. In the catalytic activity measurements, it is aimed that the NiO phase is reduced to the metallic Ni phase, and the Co_3O_4 phase is present in the form of cobalt oxide. The results obtained from the TPR–H_2 measurements showed that after in situ reduction of the catalysts before catalytic activity, nickel was in the form of the metallic nickel phase and Co_3O_4 was in the form of the CoO phase.

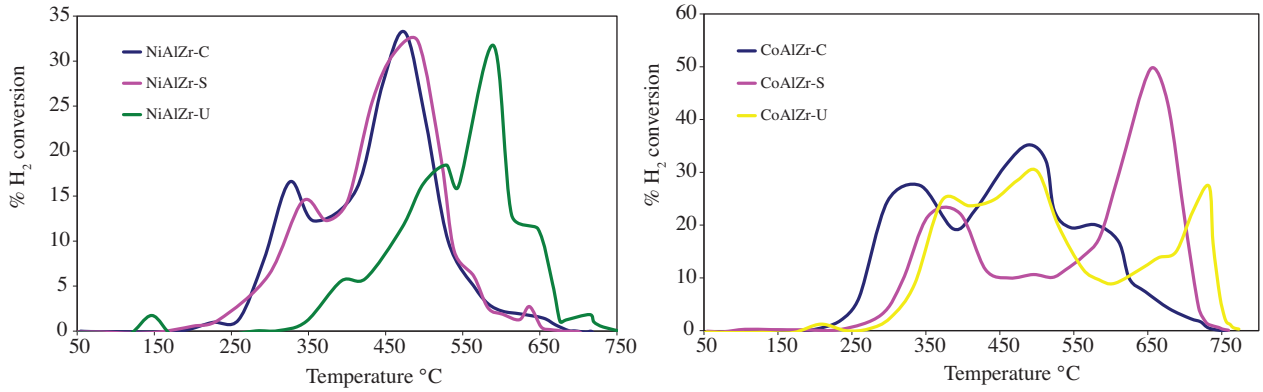

Figure 3. TPR–H_2 profiles of the CoAlZr and NiAlZr catalysts.

SEM micrographs were obtained with the CoAlZr–U and NiAlZr–U catalysts (Figure 4). The reported studies explained that Al_2O_3 presented spongy, irregularly shaped large blocks and ZrO_2 presented tubular like particles.[41,42] When CoAlZr–U catalysts are considered, it is observed that the morphology of the catalyst is different from that of the single ZrO_2 and single Al_2O_3 catalysts. The large blocks and tubular like structures of the Al_2O_3 and ZrO_2 were changed to small particles and the gaps between the particles were small. The surface morphology of the NiAlZr–U catalyst is distinctly different from that of the CoAlZr–U catalyst. The NiAlZr–U catalyst showed the typical eutectic microstructure.[43] This microstructure is formed by an intergrowth of ZrO_2 lamellae in a continuous Al_2O_3 matrix.[43] The SEM photographs showed that the catalysts' preparation method did not significantly affect the shape or size of the particles. The weight percentages of components obtained

from the EDX analysis are given in Table 2. When considering NiAlZr catalysts, the obtained weight percentages are close to the desired weight percentage. While the obtained cobalt weight percentages are greater than the desired weight percentage, the Al and Zr weight percentages are smaller than the desired weight percentages.

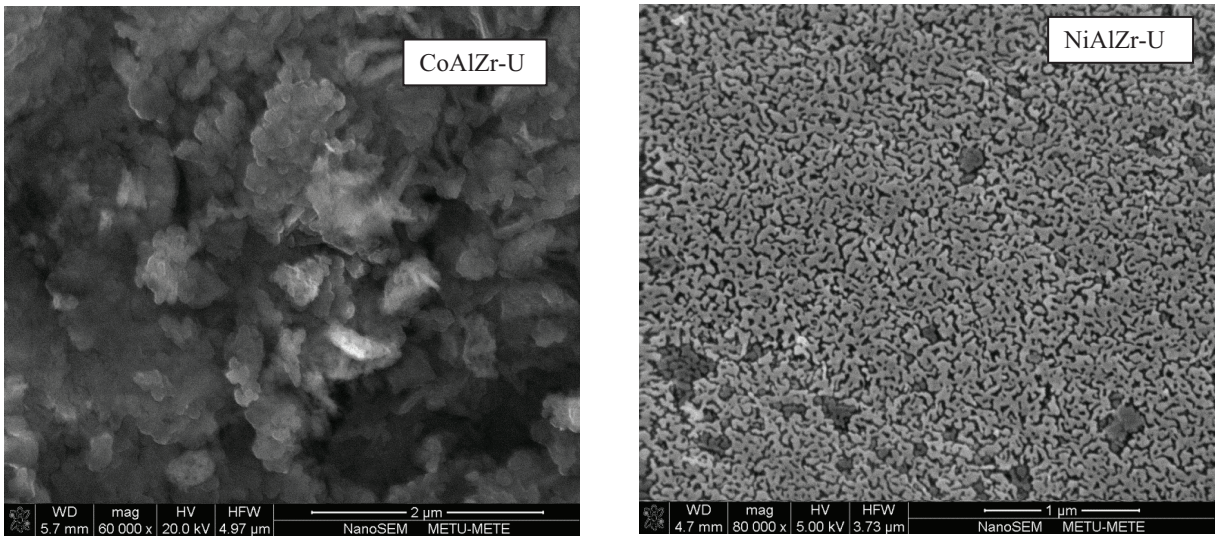

Figure 4. SEM images of the catalysts SEM images of the catalysts prepared by surfactant assisted co-precipitation with ultrasound mixing.

Table 2. SEM-EDX analysis of the catalysts.

Catalysts	Preparation method	Ni	CoK	Al	ZrL
$NiO–Al_2O_3–ZrO_2$	C	55.23	-	24.29	20.48
	S	48.70	-	26.62	24.60
	U	47.71	-	26.38	25.91
$Co_3O_4–Al_2O_3–ZrO_2$	C	-	64.80	25.49	9.71
	S	-	73.90	13.68	12.42
	U	-	72.27	15.32	12.41

The morphology of the NiAlZr and CoAlZr catalysts, which were prepared by surfactant-assisted co-precipitation, is shown in Figure 5. From the TEM image of the CoAlZr catalyst, large particles and some surface agglomerations are observed. The TEM image of the NiAlZr catalyst shows that NiO crystallites are well distributed in comparison with the cobalt oxide particles in the CoAlZr.

2.2. Catalytic activity results

Catalytic activity results of the catalysts for the CO methanation and selective CO methanation reactions are given in this section. Since the aim of using the catalyst was to eliminate the CO in the reformer gas, which was the hydrogen-rich gas, catalytic activity studies for the CO and selective CO methanation reactions were carried out. The CO methanation reactions were performed between 125 °C and 375 °C. All catalysts were in situ reduced before the methanation reactions by using pure H_2 gas at 500 °C for 1 h. After cooling down to room temperature, a CO- and H_2-containing feed was injected. Catalytic activities of the catalysts as a function of the reaction temperature for the CO methanation reaction are shown in Figures 6 and 7 and conversion temperatures (50% and 100%) are shown in Table 3.

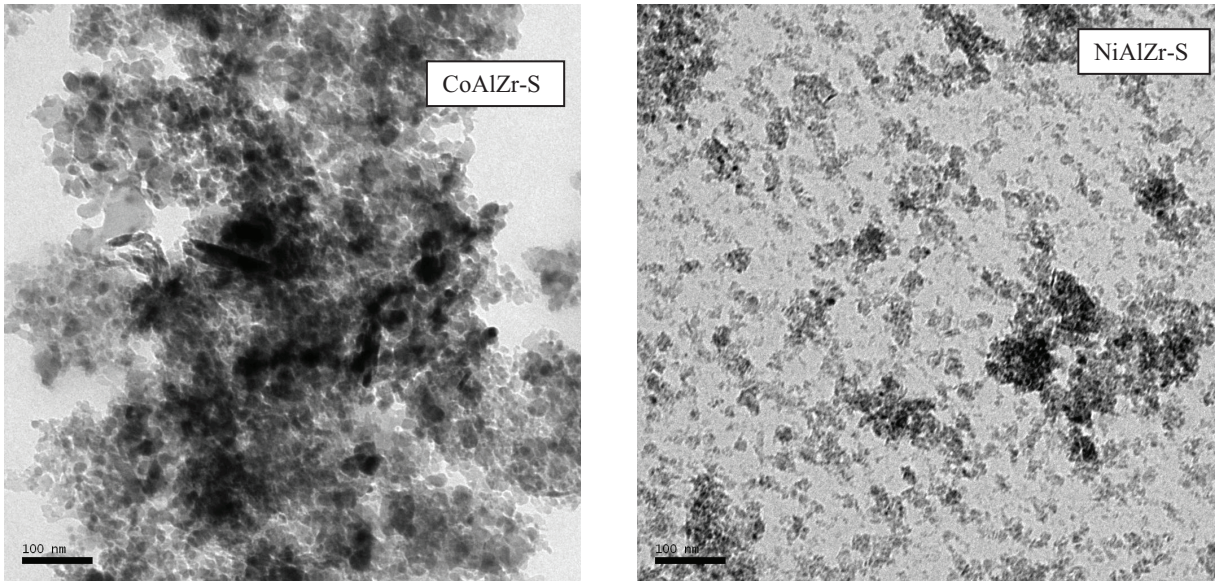

Figure 5. TEM images of the catalysts prepared by surfactant assisted co-precipitation.

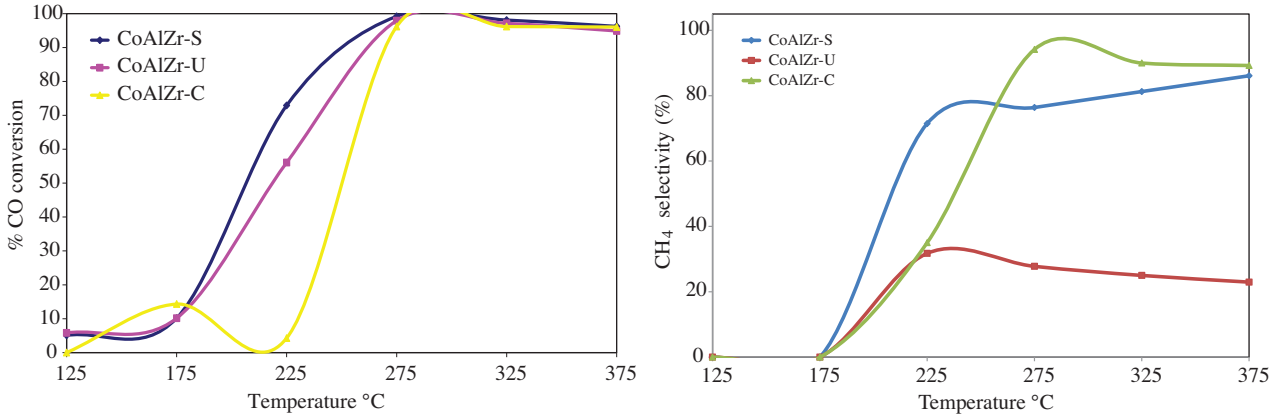

Figure 6. Activity results as a function of the temperature for CO methanation over the CoAlZr catalysts (1% CO, 50% H_2, and remainder He; S.V.: 45,000 h^{-1}; 25 mg of catalysts).

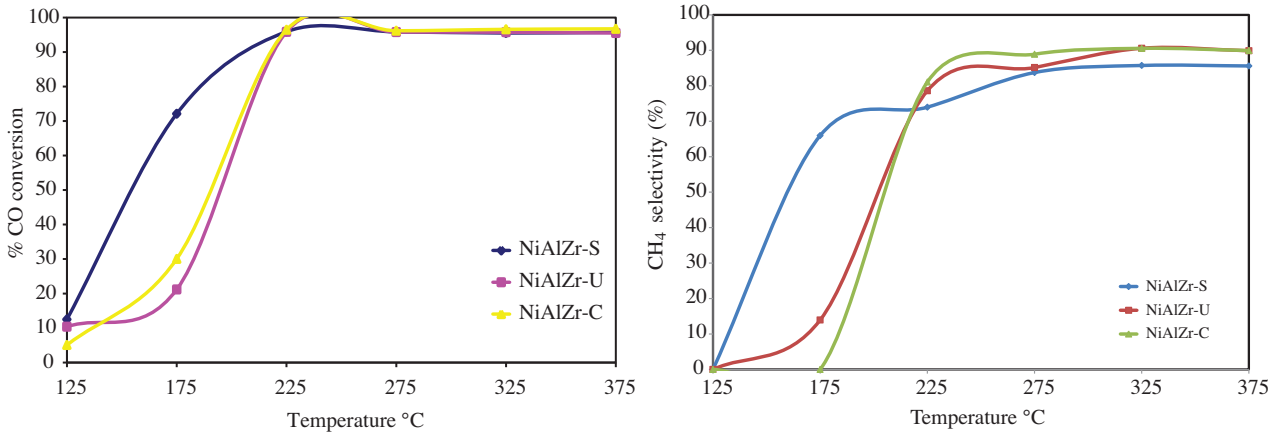

Figure 7. Activity results as a function of the temperature for CO methanation over the NiAlZr catalysts (1% CO, 50% H_2, and remainder He; S.V.: 45,000 h^{-1}; 25 mg of catalysts).

Table 3. The CO conversion temperatures of the catalysts obtained from CO methanation activity tests.

Catalysts	Preparation method	50% CO conversion temperature ($T_{1/2}$)	100% CO conversion temperature
NiAlZr	C	191 °C	T > 225 °C
	S	155 °C	
	U	196 °C	
CoAlZr	C	251 °C	T > 275 °C
	S	207 °C	
	U	218 °C	

The CO methanation catalytic activity results of the CoAlZr catalysts are shown in Figure 6. Among the CoAlZr catalysts, the lowest 50% CO conversion temperature was obtained from the CoAlZr–S catalyst. The 50% CO conversion temperatures of the CoAlZr–S, CoAlZr–U, and CoAlZr–C can be arranged as 207 °C, 218 °C, and 251 °C, respectively. All CoAlZr catalysts show 90% CO conversion after 275 °C. The shapes of the CH_4 formation curves obtained over the CoAlZr catalysts are similar to each other. All CO converted to CH_4 after 275 °C. The CH_4 formation over the CoAlZr–S catalyst was fast. Within the CoAlZr catalysts, surfactant-assisted co-precipitation can be specified as the most effective preparation method. To prepare the catalyst with ZrO_2 might improve the activity because CoAlZr catalysts show 100% CO conversion at lower temperature than that stated by Batitsa et al., who observed 90% CO conversion to CH_4 at 400 °C over Co/γ–Al_2O_3 catalyst.[44] Takenaka et al. studied CO methanation over Co-supported catalysts at 573 K. The highest CO methanation activity was observed over the Co/Al_2O_3 catalyst between the $CoSiO_2$, $CoZrO_2$, and $CoTiO_2$ catalysts.[45] At 573 K, CoAlZr catalysts prepared in the present study gave 100% CO conversion to methane.

The CO methanation catalytic activity results of the NiAlZr catalysts are shown in Figure 7. As seen from the figures, 50% CO conversion temperatures of the NiAlZr catalysts are lower than those of the CoAlZr catalysts. The NiAlZr–S catalyst has the lowest 50% CO conversion temperature (155 °C). The 50% CO conversion temperatures of the NiAlZr–C and NiAlZr–U catalysts are higher than those of the NiAlZr–S catalysts. The NiAlZr–U gave 50% CO conversion at 196 °C and NiAlZr–C gave 50% CO conversion at 191 °C. The good activity observed from NiAlZr catalysts might be connected with the Ni and typical eutectic microstructures of the catalysts. All NiAlZr catalysts gave 100% CO conversion at T > 225 °C. CO_2 was not observed during the reaction in the effluent gas mixture, which indicated that all CO was used for the methanation reaction. Comparing with the data given by Choudhury et al., who studied CO methanation over Ni–La_2O_3–Ru–Rh–θ–Alumina and obtained 50% CO conversion at 225 °C,[46] in our study NiAlZr catalysts show higher CO conversion, close to 100% at 200 °C.

The % CH_4 selectivities of the CoAlZr catalysts are shown in Figure 6. Until 175 °C, CoAlZr catalysts did not show any CH_4 selectivity. According to the CH_4 selectivity results, the most active catalyst is CoAlZr–S. However, 100% CH_4 selectivity was not observed over the CoAlZr catalysts. The highest CH_4 selectivity was observed over the CoAlZr–C catalyst. The CoAlZr–U catalyst showed maximum ≈30% CH_4 selectivity at 225 °C and CH_4 selectivity decreased after 225 °C. Although all CoAlZr catalysts gave 100% CO conversion after 275 °C, 100% CH_4 selectivity was not observed at this temperature. These results indicated that CO might be adsorbed onto the active sites of the CoAlZr catalyst in order to form the carbonate species since no CO_2 was observed in the effluent gas stream. The % CH_4 selectivity to CO methanation results obtained over the NiAlZr catalysts are shown in Figure 7. The CH_4 selectivities of the NiAlZr catalysts increased with

increasing temperature. All NiAlZr catalysts gave ≈90% CH_4 selectivity at temperatures higher than 250 °C. These results indicated that CO methanation was completed at 250 °C. The NiAlZr–S catalyst gave up to 60% selectivity at 175 °C, which was higher than the values obtained over NiAlZr–C and NiAlZr–U catalysts. According to the CH_4 selectivity results, NiAlZr catalysts are more active than the CoAlZr catalysts and NiAlZr–S has the highest CO methanation activity.

These activity results might be connected with the characterization results. Although surface area was not directly proportional to catalytic activity, the highest catalytic activity results were obtained over the catalysts that had high surface area values in this study. The catalysts of which the preparation includes the surfactant have high surface area and uniform pore size distribution. As a result, these catalysts gave good activity for the methanation reaction. According to the results obtained from the temperature programmed reduction studies, after in situ reduction of the NiAlZr and CoAlZr catalysts, the metallic nickel phase and cobalt oxide phase were present in the catalysts' structure, respectively. The good activity obtained from the NiAlZr catalyst was a result of the metallic nickel phase. Since an effect of cobalt oxide on the methanation activity of the catalysts was aimed, the cobalt oxide phase was not reduced to the metallic cobalt phase. Since cobalt was in the form of the cobalt oxide phase after in situ reduction, less activity was obtained from the CoAlZr catalysts than the NiAlZr catalysts. According to the TEM measurements, the nickel oxide particles were better distributed in NiAlZr catalysts than the cobalt oxide particles in the CoAlZr catalyst. It is known that catalytic activity mostly depends on the active site distribution in the catalyst's structure. Therefore, more distribution leads to more catalytic activity. As a result, NiAlZr catalysts showed better activity than the CoAlZr catalyst.

The aim of the present study was to reduce the CO in the reformer gas in order produce H_2-rich fuel for PEMFC by selective methanation. Therefore, a selective methanation activity test was carried out. The selective CO methanation catalytic activity tests were done over the NiAlZr–S catalysts, which showed the best catalytic activity for CO methanation. A feed composed of 1% CO, 25% CO_2, 50% H_2, and the remainder He was used and the reaction temperature was increased from 100 °C to 600 °C.

The selective CO methanation activity results are shown in Figure 8. The results indicated that all CO converted the CH_4 up to 200 °C. After this temperature, CO concentration increased again by increasing the reaction temperature. This would be due to the reverse water gas shift (RWGS) reaction, which is thermodynamically favored at higher temperatures. The RWGS reaction occurred because of the relatively high CO_2 concentration.[47] If CO_2 methanation and RWGS reactions occurred, significantly hydrogen loss might occur. After 200 °C, the increases in CO and CH_4 concentrations were mostly due to the CO_2 methanation and RWGS reactions.[48] The NiAlZr–S did not catalyze the CO/CO_2 methanation reaction but promoted conversion of CO_2 to CO via the RWGS reaction. The CO/CO_2 methanation reaction temperature was suggested to be in the range of 100–200 °C in order to convert CO to CH_4. While no CO_2 conversion occurred, 0.69% and 0.05% CO molar % were obtained at 100 °C and 200 °C, respectively. The selective CO methanation results are supported by Panagiotopoulou et al., who investigated co-methanation over Ru-, Rh-, Pd-, and Pt-supported Al_2O_3 catalysts. They observed that Pt-supported Al_2O_3 catalysts catalyzed the RWGS reaction during co-methanation.[49]

In the present study, NiO–Al_2O_3–ZrO_2 and Co_3O_4–Al_2O_3–ZrO_2 catalysts were prepared by three different co-precipitation methods (co-precipitation, surfactant-assisted co-precipitation, and surfactant-assisted co-precipitation with ultrasound mixing). According to the results, the effects of the surfactant and ultrasound were determined. Catalysts prepared by surfactant-assisted co-precipitation gave higher surface area values than conventional co-precipitation. Compared to mechanical mixing, the surface area values of the catalysts were not significantly changed by using ultrasound mixing. The effect of the surfactant on the surface area

value of the NiAlZr catalyst is very significant. The surfactant leads to catalysts with smaller pore diameters and higher pore volumes. Temperature programmed reduction (TPR–H_2) analysis showed that the surfactant led to an increase in the resistance to hydrogen reduction of the catalysts. The reduction temperatures shifted to higher values. The catalytic activities of the catalysts for the CO methanation and selective CO methanation reactions were determined. The CO methanation activity results showed that CoAlZr and NiAlZr catalysts gave high activities. Over the NiAlZr catalysts, all CO converted to CH_4 at $\approx$225 °C. Since all catalysts were in situ reduced under 100% H_2 before the reaction, CO_2 was not observed in the effluent gas mixture. Selective CO methanation was carried out over the NiAlZr–S catalyst. After 300 °C methanation activity decreased because of the reverse water gas shift reaction. The CO level decreased under 100 ppm at 200 °C.

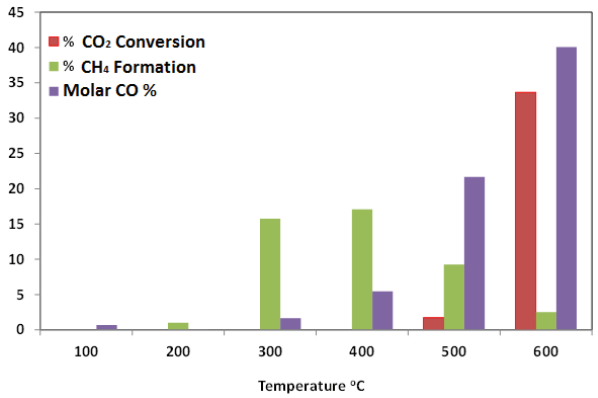

Figure 8. Activity results as a function of the temperature for selective CO methanation over the NiAlZr–S (1% CO, 25% CO_2, 50% H_2, and remainder He; S.V.: 45,000 h^{-1}; 25 mg of catalysts).

3. Experimental

The 50/25/25 (mol %) NiO–Al_2O_3–ZrO_2 and 50/25/25 (mol %) Co_3O_4–Al_2O_3–ZrO_2 catalysts were prepared by three different methods, which are described below. The method that we used is given by Derekaya et al.[50] Characteristic properties were determined by different techniques. Finally, methanation studies were carried out to investigate the effect of the catalyst preparation methods on activity.

3.1. Catalyst preparation

3.1.1. Co-precipitation

$Ni(NO_3)_2.6H_2O$ (Aldrich, 99.8%), $Co(NO_3)_2.6H_2O$ (Fluka, 99.0%), and $Zr(NO_3)_2.xH_2O$ (Sigma, 99%) were dissolved in distilled water to adjust them to the desired molar ratios. Total concentration of the metals in the final aqueous solution was 0.1 M. The metal salt solution and required amount of Al_2O_3 (mesoporous) were put into a stirrer. Na_2CO_3 (1 M) solution was added to the solution to adjust its pH to 8. The precipitates were aged for 3 h at pH 8, and then filtered and washed with hot distilled water several times in order to remove excess ions. They were air dried overnight at 110 °C. Finally, catalysts were calcined in air at 500 °C for 3 h. The co-precipitation technique was designated as "C".

3.1.2. Surfactant-assisted co-precipitation

First 6 mmol of cetiyltrimethylammoniumbromide (CTAB) was dissolved in 200 mL of deionized water for 15 min by using a mechanical stirrer. Then the desired amount of metal salt solution was added to the CTAB

solution under vigorous stirring. After this solution was mixed for 0.5 h, sodium hydroxide solution was added at 0.2 mol/L flow rate until the pH value of the solution reached 10. Then the solution was mixed for 12 h and the precipitate was aged for 3 h at 90 °C. Next it was filtered and washed with hot distilled water several times in order to remove excess ions. They were air dried overnight at 110 °C. Finally, the catalysts were calcined in air at 500 °C for 3 h. The surfactant-assisted co-precipitation technique was designated as "S".

3.1.3. Surfactant-assisted co-precipitation with ultrasound mixing

First 6 mmol of cetiyltrimethylammoniumbromide (CTAB) was dissolved in 200 mL of deionized water for 15 min by using an ultrasound stirrer. Then the desired amount of metal salt solution was added to the CTAB solution under vigorous stirring. After this solution was mixed for 0.5 h, sodium hydroxide solution was added at 0.2 mol/L flow rate until to bring the pH of the solution to 10. After this solution was mixed for 12 h, the precipitate was aged for 3 h at 90 °C by using both mechanical and ultrasound stirrers. The stirring time was adjusted as 20 min ultrasound stirrer + 40 min mechanical stirrer + 20 min ultrasound stirrer + 40 min mechanical stirrer + 20 min ultrasound stirrer + 40 min mechanical stirrer. Then the precipitates were filtered and washed with hot distilled water several times in order to remove excess ions. They were air dried overnight at 110 °C. Finally, the catalysts were calcined in air at 500 °C for 3 h. The surfactant-assisted co-precipitation with ultrasound mixing technique was designated as "U".

3.2. Catalyst characterization

Different techniques were used in order to determine the physical properties of the catalysts, namely X-ray diffraction (XRD), X-ray photoelectron spectroscopy (XPS), N_2 adsorption, thermogravimetric analysis (TGA), temperature programmed reduction (TPR–H_2), scanning electron microscopy (SEM), and high resolution transmission electron microscopy (HRTEM). BET, multipoint surface areas, pore volumes, and pore diameters of the catalysts were evaluated by a Quantochrome Autosorp 1C/MS device. Before the analysis, samples were outgassed at 300 °C for 1 h. Average pore sizes were determined by the BJH method. X-ray diffraction patterns were obtained using a PHILIPS PW 1840 diffractometer. A Rigaku rotating anode X-ray diffractometer system generating CuKα radiation was used to obtain XRD patterns. The oxidation states of the components in the catalyst structure were determined by XPS. The XPS patterns of the catalysts were obtained by using a PHI5000 device, which had an AlKα monochromatic anode at the 600 W X-ray power source. Fresh catalysts, calcined at 500 °C, were used in this analysis. Temperature programmed reduction was carried out by a PerkinElmer Clarus 500 gas chromatograph equipped with a thermal conductivity detector (TCD). In each experiment 25 mg of catalysts was used. Before the reduction, catalyst samples were pretreated with He at 500 °C for 1 h. TPR measurement was performed after cooling the samples to room temperature in the helium flow. A gas mixture of 5% H_2 and 95% N_2 was used with a flow rate of 50 mL/min, while the reactor was heated from room temperature to 800 °C at a heating rate of 10 °C/min. Catalyst morphology was examined using a NOVA NANOSEM 430 device. The catalyst surface morphology and the metal dispersion on the surface were determined by TEM analysis. The TEM measurements were carried out on a JEOL 2100 HRTEM electron microscope.

3.3. Activity measurements

Catalytic activities of the catalysts were determined for the methanation reactions. All of the catalysts were tested for CO methanation activity and the catalysts showing the lowest 50% CO conversion temperature were

further tested for selective CO methanation activity. Before the catalytic measurements, fresh catalysts were in situ reduced under 100% H_2 atmosphere for 1 h at 500 °C. Catalytic activity measurements for the CO methanation reaction were carried out in a fixed bed quartz tubular reactor using 25 mg of catalyst. A 1% CO, 50% H_2, and remainder He feed gas composition was used. The temperature of the reactor was changed from 125 °C to 375 °C. The flow rate of the feed gas was 25 mL/min. The analysis of the reactor effluent was performed by an online PerkinElmer CLARUS 500 gas chromatograph equipped with a TCD. The chromatograph column packing was carbosphere and the column temperature was maintained at 50 °C. The selective CO methanation reaction was performed using a feed gas with a composition of 1% CO, 25% CO_2, 50% H_2, and remainder He while the reactor temperature was changed from 100 °C to 600 °C.

The CO, CO_2, and H_2 conversions were calculated using the equations given below:

For the CO methanation: % CO conversion $= \frac{[CO]_0-[CO]_f}{[CO]_0} \times 100$

For the CO_2 methanation: % CO_2 conversion $= \frac{[CO_2]_0-[CO_2]_f}{[CO_2]_0} \times 100$

For the CH_4 selectivity: % CH_4 selectivity $= \frac{[CH_4]_{0ut}}{[CO]_0-[CO]_f} \times 100$,

where $[CO]_0$ = the inlet CO concentration in the feed gas; $[CO]_f$ = the outlet CO concentration; $[CO_2]_0$ = the inlet CO_2 concentration in the feed gas; $[CO_2]_f$ = the outlet CO_2 concentration; $[CH_4]_{out}$ = the outlet CH_4 concentration.

Acknowledgments

The authors gratefully acknowledge the financial support from the Gazi University BAP 18/2008-01 and TÜBİTAK 109M230 projects.

References

1. Habazaki, H.; Yamasaki, M.; Zhang, B. P.; Kawashima, V.; Kohno, S.; Takai, T.; Hashimoto, K. *Appl. Catal. A-Gen.* **1998**, *172*, 131–140.
2. Ma, S.; Tan, Y.; Han, Y. *J. Nat. Gas. Chem.* **2011**, *20*, 435–440.
3. Zhao, A.; Ying, W.; Zhang, H.; Ma, H.; Fang, D. *Catal. Commun.* **2012**, *17*, 34–38.
4. Hwang, S.; Hong, U. G.; Lee, J.; Seo, J. G.; Baik, J. H.; Koh, D. J.; Lim, H.; Song, I. K. *J. Ind. Eng. Chem.* **2013**, *19*, 2016–2021.
5. Hwang, S.; Lee, J.; Hong, U. G.; Baik, J. H.; Koh, D. J.; Lim, H.; Song, I. K. *J. Ind. Eng. Chem.* **2013**, *19*, 698–703.
6. Jia, C.; Gao, J.; Gu, F.; Xu, G.; Zhong, Z.; Su, F. *Catal. Sci. Technol.* **2013**, *3*, 490–499.
7. Hu, D.; Gao, J.; Ping, Y.; Jia, L.; Gunawan, P.; Zhong, Z.; Xu, G.; Gu, F.; Su, F. *Ind. Eng. Chem. Res.* **2012**, *51*, 4875–4856.
8. Ma, S.; Tan, Y.; Han, Y. *J. Ind. Eng. Chem.* **2011**, *17*, 723–726.
9. Chen, B.; Falconer, J. L.; Bailey, K. M.; Sen, B. *Appl. Catal.* **1990**, *66*, 283–300.
10. Tsoncheva, T.; Ivanova, L.; Rosenholm, J.; Linden, M. *Appl. Catal. B- Environ.* **2009**, *89*, 365–374.
11. Guo, C.; Wu, Y.; Qin, H.; Zhang, J. *Fuel Process. Techn.* **2014**, *124*, 61–69.
12. Gomez, L. E.; Tiscornia, I. S.; Boix, A. V.; Mirs, E. E. *Appl. Catal. A-Gen.* **2011**, *401*, 124–133.
13. Ma, C.; Yao, N.; Han, Q.; Li, X. *Chem. Eng. J.* **2012**, *191*, 534–540.
14. Ma, S.; Tan, Y.; Han, Y. *J. Ind. Eng. Chem.* **2011**, *17*, 723–726.

15. Kok, E.; Scott, J.; Cant, N.; Trimm, D. *Catal. Today* **2011**, *164*, 297–301.
16. Yaccato, K.; Carhart, R.; Hagemayer, A.; Lesik, A.; Strasser, P.; Volpe Jr., A. F.; Turner, H.; Weinberg, H.; Graselli, R. K.; Brooks, C. *Appl. Catal. A. Gen.* **2005**, *296*, 30–48.
17. Zhao, A.; Ying, W.; Zhang, H.; Ma, H.; Fang, D. *J. Nat. Gas. Chem.* **2012**, *21*, 170–177.
18. Balıkçı, F.; Yüceer, S. B.; Güldür, Ç. *Chem. Eng. Commun.* **2009**, *196*, 171–181.
19. Balıkçı, F.; Güldür, Ç. *J. Chem.* **2007**, *31*, 465–471.
20. Liu, W. J.; Zeng, F. X.; Jiang, H.; Zhang, X. S.; Li, W. W. *Chem. Eng. J.* **2012**, *180*, 9–18.
21. Gac, W. *Catal. Today* **2011**, *176*, 131–133.
22. Lin, S. S. Y.; Daimon, H.; Hu, S. Y. *Appl. Catal. A- Gen.* **2009**, *366*, 252–261.
23. Chu, Z.; Chen, H.; Yu, Y.; Wang, Q.; Fang, D. *J. Molec. Catal. A-Chem.* **2013**, *366*, 48–53.
24. Soleimani, S.; Salabat, A.; Tabor, R. F. *J. Colloid. Interface Sci.* **2014**, *426*, 287–292.
25. Simanjuntak, F. S. H.; Lim, S. R.; Ahn, B. S.; Kim, H. S.; Lee, H. *Appl. Catal. A-Gen.* **2014**, *484*, 33–38.
26. Khosbin, R.; Haghighi, M. *Chem. Eng. Res. Design.* **2013**, *91*, 1111–1122.
27. Zhou, X.; Chen, Q.; Tao, Y.; Weng, H. *J. Catal.* **2011**, *37*, 1156–1165.
28. Asencios, Y. J. O.; Assaf, E. M. *Fuel Process. Technol.* **2013**, *106*, 247–252.
29. Khaodee, W.; Jongsomjit, B.; Assabumrungrat, S.; Praserthdam, P.; Goto, S. *Catal. Commun.* **2007**, *8*, 548–556.
30. Fischer, N.; Van Steen, E.; Claeys, M. *Catal. Today* **2011**, *171*, 174–179.
31. Sing, K. S. W.; Everett, D. H.; Haul, R. A. W.; Moscou, L.; Pierotti, R. A.; Rouquerol, J.; Siemieniewska, T. *Int. Union Pure Appl. Chem.* **1985**, *57*, 603–619.
32. Hagelin-Weaver, H. A.; Hoflund, G. B.; Minahan, D. M.; Salaita, G. N. *Appl. Surf. Sci.* **2004**, *235*, 420–488.
33. Jiang, H.; Meng, X.; Dai, H.; Deng, J.; Liu, Y.; Zhang, L.; Zhao, Z. *J. Hazard. Mater.* **2012**, *217–218*, 92–99.
34. Xuehong, Z.; Rui, W.; Licheng, L.; Honxing, D.; Guizhen, Z.; Hang, H. *Chinese J. Catal.* **2011**, *32*, 827–835.
35. Hernandez, M. L.; Montoya, J. A.; Del Angel, P.; Hernandez, I.; Espinosa, G.; Lianoz, M. E. *Catal. Today* **2006**, *116*, 169–178.
36. Richter, M.; Langpape, M.; Kolf, S.; Grubert, G.; Eckelt, R.; Radnik, J.; Schneider, Pohl, M.; Frice, R. *Appl. Catal. B- Environ.* **2000**, *36*, 73–81.
37. Ashok, J.; Raju, G.; Reddy, P. S.; Subrahmanyam, M.; Venugopal, A. *Int. J. Hydrogen Energ.* **2008**, *33*, 4809–4818.
38. Dajiang, M.; Yaoqiang, C.; Junber, Z.; Zhenling, W.; Di, M.; Maochu, G. *J. Rare Earth.* **2007**, *25*, 311–315.
39. Abbasi, Z.; Haghighi, M.; Fatehifar, E.; Saedy, S. *J. Hazard. Mater.* **2011**, *186*, 1445–1454.
40. Lin, S. S. Y.; Kim, D. H.; Engelhard, M. H.; Ha, S. Y. *J. Catal.* **2010**, *273*, 229–235.
41. Liotta, L. F.; Di Carlo, G.; Pantaleo, G.; Deganello, G. *Catal. Commun.* **2005**, *6*, 329–336.
42. Zhang, D.; Duan, A.; Zhao, Z.; Wan, G.; Gao, Z.; Jiang, G.; Chi, K.; Chuang, K. H. *Catal. Today.* **2010**, *149*, 62–68.
43. Rekha, M.; Manjunath, H. R.; Nagaraju, N. *J. Ind. Eng. Chem.* **2013**, *19*, 337–346.
44. Miyoshi, K.; Farmer, S. C.; Sayir, A. *Tribol. Int.* **2009**, *38*, 974–986.
45. Batista, M. S.; Santiago, E.; Assaf, E. M.; Ticianelli, E. A. *J. Power Sources* **2005**, *145*, 50–54.
46. Takenaka, S.; Shimizu, T.; Otsuka, K. *Int. J. Hydrogen Energ.* **2004**, *29*, 1065–1073.
47. Choudhury, M. B. I.; Ahmed, S.; Shalabi, M. A.; Inui, T. *Appl. Catal. A-Gen.* **2006**, *314*, 47–53.
48. Liu, Q.; Liao, L. W.; Dong, X. *J. Nat. Gas. Chem.* **2010**, *19*, 497–502.
49. Zyryanova, M. M.; Snytnikov, P. V.; Amosov, Y. I.; Kuzmin, V. A.; Kirilov, V. A.; Sobyanin, V. A. *Chem. Eng. J.* **2011**, *176–177*, 106–113.
50. Derekaya, B. F.; Mercan, D. *Turk. J. Chem.* **2014**, *38*, 568–580.